Geophys. J. R. astr. Soc. (1982) **70**, 503–527

Dispersion and attenuation of mantle waves through waveform inversion

Adam M. Dziewonski and Joseph M. Steim *Department of Geological Sciences, Harvard University, Cambridge, Massachusetts 02138, USA*

Received 1982 January 20; in original form 1981 August 11

Summary. We propose a new approach to the determination of elastic and anelastic parameters of the Earth's structure from seismic data. Instead of measuring such functionals of the medium response as the phase delay or spectral ratios, we perturb parameters of the model to satisfy the observed waveforms. The advantage of our waveform inversion technique (WIT) is that it uses the properties of the Earth as a smoothing filter. Also, because the Earth's structure is the common denominator, the method allows simultaneous interpretation of different functionals of this structure; for example, the waveforms of Rayleigh and Love waves for the same source-receiver pair.

Following extensive testing of the method on synthetic and actual data, we subject results of our analysis of 37 recordings for various sources and stations to 'pure path' decomposition. The period range of analysis extends from 160 to 630 s. We distinguish four types of regions: stable continents, areas tectonically active within the last 400 Myr, ocean floors younger than 38 Myr, and old ocean floors older than 38 Myr.

The results indicate significantly different responses of the oceanic and continental areas at long periods. Stable continental and tectonic regions have nearly the same dispersion for periods greater than 300–350 s, and then diverge rapidly, with stable continents showing higher velocities. The young and old oceans, on the other hand, become distinct at periods as long as 500 s; the old oceans are faster. In terms of shear velocity models, the data are consistent with a difference of about 4 per cent between the young and old oceans in a depth range from 400 to 670 km, while the continental regions are similar and close to the global average. At shallower depths our structures are conceptually similar to those inferred from previous 'pure path' analyses and short-period surface wave studies.

While we cannot, yet, establish statistically significant differences in Q for the four regions, such differences are obtained if one distinguishes only between continents and oceans: the Q for the latter is 10–20 per cent lower in the period range of the analysis.

1 Introduction

Measurement of dispersion and attenuation of mantle waves (fundamental spheroidal and toroidal modes with sufficiently long periods that their wavegroups are discernible beyond the first minor and major arc arrivals) is one of the classical problems in seismology. Probably the work of Satô (1958) represents the first step toward the modern methods of analysis of these waves. Satô noticed that by estimating the difference between the phase delay functions of two arrivals, whose paths differ by one circumference of the Earth, at the same station one can measure the phase velocity without the need to correct the data for instrumental response and source phase shift. Unfortunately, in his calculations Satô did not account for the polar phase shift (Brune, Nafe & Alsop 1961) and, therefore, his results were wrong by a factor $(l + 1/2)/l$, where l is the angular order number. Satô also measured the attentuation factor by evaluating the spectral ratio R_{n+2}/R_n at a number of frequency intervals. Many papers on dispersion and attenuation of mantle waves utilized Satô's approach; Kanamori (1970), in addition to his own measurements, summarized most of the data published through the 1960s.

Dziewonski & Landisman (1970) proposed an auto-correlation technique, whose advantage is the improvement in signal-to-noise ratio due to simultaneous consideration of the signal from all the appropriate pairs of wavegroups present in a recording of a major earthquake. Dziewonski, Mills & Bloch (1972) developed the 'residual dispersion technique', which allows one to eliminate most of the dispersion present in a particular wavegroup arrival. This is accomplished by cross-correlation of the observed signal with a unit-amplitude synthetic seismogram calculated for a reference earth model. Thus, one can achieve contraction of the signal in time, reduce the difficulty caused by interference of waves propagating with different velocities and, in general, improve the signal-to-noise ratio. This approach has been used, for example, by Sailor (1978) in his study of Q of mantle waves.

Nakanishi (1979) derived filters (transfer functions) which simultaneously describe dispersion and attenuation of mantle waves. Our technique is similar, but the details are quite different conceptually and numerically.

One of the principal difficulties of all previous techniques lies in the need to isolate the time traces associated with the arrivals of individual wavegroups. It usually involves truncation of the signal outside a certain range of group velocities. This limits the range of periods in which dispersion and attenuation can be measured, as well as introduces some distortion of the spectra, particularly severe near the upper limit of periods of interest. For these reasons, reliable measurements generally do not extend beyond 300 s.

The approach involving observation of periods of normal modes avoids this difficulty. Silver & Jordan (1981) published results of their analysis of the normal mode spectra using the moment-ratio approach of Jordan (1978). The method works well at long periods; below 250–200 s the spectral peaks are less clearly defined and interference of overtones becomes severe. The precision of the data of Silver & Jordan is impressive; they achieve accuracy sufficient to resolve the differences in local frequencies (Jordan 1978) for six types of tectonic regions.

Several methods of measuring attenuation of normal modes have been proposed in the literature, but there are severe difficulties at periods shorter than 500–300 s and the spread of published data is very large.

In what follows, we describe an approach to the estimation of dispersion and attenuation of mantle waves. By using perturbation theory we avoid the direct measurement of those quantities but, instead, we modify a reference (starting) earth model in such a way that the transfer function computed for this new model satisfies the data in the least squares sense. We call this method waveform inversion technique (WIT).

After the method is tested on synthetic and actual data, we apply it to the analysis of recordings from the International Deployment of Accelerometers network (IDA; see Agnew *et al.* 1976) and derive 'pure path' (or 'local', after Jordan 1978) normal mode periods and attenuation in a range from 160 to 600 s. Statistically significant differences are obtained for the Q characteristic of continental and oceanic regions: waves travelling along oceanic paths are attenuated more rapidly.

However, the inferences with respect to the local structures consistent with these data must be made with caution, at this stage. Future implementation of the theory proposed by Woodhouse & Girnius (1982) should allow for the fact that the waves of different lengths sample the Earth differently and, in particular, that as the wavelength increases, the averaging kernels sample a greater proportion of the entire Earth, leading to the breakdown of the approximation implicit in geometrical ray theory.

2 The waveform inversion technique (WIT)

As stated above, the principle of measuring phase velocity and attenuation from observations of mantle waves is very simple. The spectral ratio of two wavegroups whose paths differ by one circumference yields the spectrum of the transfer function $T(\omega)$, that corresponds in the time domain to the shape of a δ-function signal after one complete passage around the Earth (Dziewonski & Landisman 1970):

$$T(\omega) = R_{n+2}(\omega)/R_n(\omega)\,. \tag{1}$$

The spectrum of $T(\omega)$ must be of the form:

$$T(\omega) = \exp\left[-\pi a\left\{i\left[2k(\omega) - \frac{1}{a}\right] + \frac{\omega q(\omega)}{2u(\omega)}\right\}\right] \tag{2}$$

where $k(\omega)$ is the (real) wavenumber, $u(\omega)$ is the group velocity, $q(\omega)$ is the inverse of the quality factor Q and a is the Earth's radius. Thus, the analysis of a phase of $T(\omega)$ allows the wavenumber to be determined as a function of frequency, and its amplitude yields $Q(\omega)$, if the group velocity is known. The frequencies of zero-crossings of the phase spectrum, defined in a $(-\pi, \pi)$ interval, correspond to the frequencies of free oscillations of the Earth.

In practice, direct application of equation (2) leads to serious difficulties. The process of deconvolution, implied by the ratio of two spectra, leads to unstable results even for a limited range of frequencies, because both spectra are contaminated by noise and energy of overtones.

Nakanishi (1979) derived $T(\omega)$ through the design of a Wiener filter, but it appears that his procedure may also lead to unstable results; the $T(\omega)$ shown in his Fig. 2(a) cannot be a functional of a realistic earth model. Clearly, the filter design process cannot distinguish between the signal and noise present in the sections of a recording associated with the R_n and R_{n+2} arrivals. The problem could be alleviated by using many pairs of arrivals simultaneously.

We intend to make use of the fact that $T(\omega)$ must be consistent with a reasonable Earth structure: all parameters in equation (2) are functionals of Earth structure, and can be readily calculated for a given earth model. Thus we plan to use the known (in general, not in detail) properties of the Earth as a smoothing filter. The most direct way to assure that this condition is satisfied is to derive the $T(\omega)$ through the process of perturbation of the structural parameters of a selected starting earth model.

We shall attempt to find a $T(\omega)$ that satisfies the following least-squares condition:

$$\int_{\omega_1}^{\omega_2} |R_{n+2}(\omega) - R_n(\omega) \cdot T(\omega)|^2 d\omega = \min . \tag{3}$$

The finite limits of integration reflect the fact that in practice high quality data are available only in a limited frequency range.

Let the $T(\omega)$ computed for the starting model be $T^0(\omega)$; it is described by a complex function $K^0(\omega)$: $T^0(\omega) = \exp[-2\pi i a K^0(\omega)]$, where:

$$K^0(\omega) = k(\omega) - \frac{1}{2a} + i\frac{\omega q(\omega)}{2u(\omega)} \tag{4}$$

thus K^0 is the complex wavenumber corrected for the effect of the polar phase shift. A small change in the structural parameters of the starting model, $\mathbf{m}^0(r, \omega)$, will lead to a change in K^0 that can be evaluated using linear perturbation theory (cf. Backus & Gilbert 1967):

$$\delta K^0(\omega) = \int_0^1 \mathbf{G}^0(r,\omega) \cdot \delta\mathbf{m}(r,\omega) dr ; \tag{5}$$

where the differential kernels, $\mathbf{G}^0$, and the change in the earth model, $\delta\mathbf{m}$, may both be complex. The effect of attenuation on velocity dispersion may be incorporated in equation (5). In examples discussed in this report, evaluation of the frequency dependence of elastic parameters is made assuming the frequency-independent Q model (cf. Liu, Anderson & Kanamori 1976), although any other relationship can be readily accommodated. Once the frequency dependence of the P- and S-velocities is stated, the model is defined at the reference frequency (we use 1 Hz) and perturbations are evaluated for the model at that frequency. Consequently, the frequency-dependent effect of $\delta\mathbf{m}$ is included, to the first order, in the differential kernels $\mathbf{G}(r, \omega)$. If the change $\delta\mathbf{m}$ is very small, then we may write:

$$\exp[-2\pi i a \delta K^0(\omega)] \sim 1 - 2\pi i a \delta K^0(\omega) = 1 - 2\pi i a \int_0^1 \mathbf{G}^0 \cdot \delta\mathbf{m} dr . \tag{6}$$

The integral over a finite frequency range in equation (3) may be changed to a sum over the discrete elements of the spectrum and, upon substitution of equation (6), the least squares condition becomes:

$$\sum_j |R_{n+2}(\omega_j) - R_n(\omega_j) T_j^0 + 2\pi i a R_n(\omega_j) \cdot T_j^0 \cdot \int_0^1 \mathbf{G}_j \cdot \delta\mathbf{m}\, dr|^2 = \min . \tag{7}$$

The inverse problem for $\delta\mathbf{m}(r)$ posed by equation (7) can be solved either in the data or parameter space using one of many methods described in the literature; it will lead to a system of equations linear in $\delta\mathbf{m}$. It is important, however, that the perturbation estimated in each iteration be small enough that the approximation assumed in equation (6) is reasonably well satisfied. Otherwise, the process may converge to a wrong solution. For this reason, it will be generally necessary to damp the inverse heavily and perform several iterations. Following each iteration $T(\omega)$ is recalculated exactly:

$$T^{(n)}(\omega) = T^{(n-1)}(\omega) \cdot \exp[-2\pi i a \delta K^{(n-1)}] . \tag{8}$$

After convergence is achieved, it is prudent to recompute the function $K(\omega)$ and the differential kernels for the improved earth model and to repeat the entire process.

As mentioned in the Introduction, another difficulty in the estimation of $T(\omega)$ is that the wavegroups corresponding to individual orbits cannot always be readily isolated. Clearly, when the receiver is close to the source or its antipodes, then the energy of odd- and even-numbered wavegroups will overlap. However, even at the optimal distance of 90°, a 500 s wave of R_5 will arrive at the same time as a 220 s wave of R_4. For this reason, the most reliable measurements of dispersion and attenuation of mantle waves have been limited to the period interval in which both Rayleigh and Love waves are weakly dispersed. The development of the technique described above, which does not require an explicit evaluation of the spectral ratio but relies on minimizing the difference between two functions of time or frequency, allows us to reformulate the approach to the analysis of mantle waves.

Consider that a synthetic seismogram consists of a series of arrivals of wavegroups: $R_1, R_2, R_3, R_4, \ldots, R_\infty$. Convolution of such a seismogram with the transfer function T, transforms it into a series: $R_3, R_4, R_5, \ldots, R_\infty$. The difference between these two series is $R_1 + R_2$, a signal of finite duration, t_1 determined by the slowest group velocity of the wavegroup R_2. The remainder of the trace is identically zero if the transfer function corresponds to the same model for which the synthetic seismogram was computed. In practice we deal with seismograms of finite duration truncated, say, at a time t_2. Let us illustrate this idea in the following diagram:

$s(t)$	R_1	R_2	¦	R_3	R_4	R_5	R_6	¦		
$s(t)*T(t)$			¦	R_3	R_4	R_5	R_6	¦	R_7	R_8
$s(t)-s(t)*T(t)$	R_1	R_2	¦	0	0	0	0	¦	$-R_7$	$-R_8$.
			t_1					t_2		

The operation described above is equivalent to:

$$s(t)*[1 - T(t)] = 0; \quad \text{for} \quad t_1 \leqslant t \leqslant t_2. \tag{9}$$

Thus, in the frequency domain, the least squares condition is:

$$\int_{\omega_1}^{\omega_2} |F[s(t)]_{t_{1,2}} - F[s(t)*T(t)]_{t_{1,2}}|^2 d\omega = \min; \tag{10}$$

where F is the Fourier transform and the subscript indicates that the transform is evaluated for the time interval from t_1 to t_2. Further procedure is identical to that described above for a pair of the wavegroups.

What has been gained is that we can use the signal contained in an entire seismogram and that we completely bypass the problem associated with the overlapping energy of wavegroups belonging to different orbits. It is not necessary that the analysed seismogram should begin with the first minor arc arrival R_1. It may begin at any time t_0, providing that the interval between t_0 and t_1 is sufficiently long; 190 min, the circumferential travel time of the slowest mantle Rayleigh waves, is a conservatively safe estimate. All the problems associated with truncation are also entirely avoided.

Furthermore, because the Earth's structure is the common denominator, a set of seismograms containing Rayleigh and Love waves may be treated simultaneously. For example, the need for introduction of anisotropy can be tested directly using waveforms from the vertical and transverse components. For seismically active regions, where many earthquakes with $M_S > 6.5$ occur within a few years, it is possible to use in a single inversion a set of seismograms from closely spaced events observed at a particular station. If these events cover a

wide range of magnitudes, this should result in broadening the range of analysis with respect to that possible for a single earthquake. Following a very large earthquake (for example, the Indonesian shock of 1977), many hours of recording are lost because of the limited dynamic range of seismic instruments, and during that time the signal with periods from 100 to 200 s may be attenuated below the noise level. For lesser events, the occurrence of non-linearity is often limited to the first minor arc arrival, and such records can be used to provide the structural constraints at higher frequencies.

The implicit assumption made in application of WIT in this report is that we consider the signal of overtones to have an effect equivalent to that of random noise. In our opinion this assumption is justified for two reasons. First, for shallow events the signal of the fundamental mode clearly dominates that due to the overtones. Secondly, and more important, the phase and group velocities of overtones differ sufficiently from those of the fundamental mode that their contribution to the difference trace $[s(t)*T(t)]_{t_1,_2}$ cannot be substantially reduced for a wide range of frequencies by small perturbations in structure. In this sense, the effect of overtones is indeed equivalent to that of random noise.

However, it is possible to design a procedure that would enhance the signal of overtones (we acknowledge here the contribution of Professor J. H. Woodhouse). Neglecting the noise, the seismogram can be represented by a sum of the signals of the fundamental mode and overtones, $o(t)$:

$$s(t) = R_1 + R_2 + R_3 + \ldots, + R_\infty + o(t).$$

But:

$$R_3 = R_1 * T, R_4 = R_2 * T, R_5 = R_1 * T * T$$

and so on; thus:

$$s(t) = (R_1 + R_2) * (1 + T + T^2 + \ldots) + o(t) = (R_1 + R_2)/(1 - T) + o(t);$$

with powers having the meaning of multiple convolution and the symbol of division that of deconvolution. Assuming that the transfer function appropriate for a given recording has been found, we can write:

$$s(t) * (1 - T) = R_1 + R_2 + o(t) * (1 - T).$$

However, $R_1 + R_2$ is zero for times greater than t_1 and therefore:

$$o(t) = \{s(t) * [1 - T(t)]\}_{t_1,_2} / [1 - T(t)]; \qquad t_2 \to \infty; \tag{11}$$

appropriate adjustments can be made for the finite truncation time. All the problems usually associated with deconvolution are avoided, because $T(t)$ is a functional of a known Earth structure and can be evaluated exactly.

Thus, in theory, it is possible to isolate the signal due to the overtones from that of the fundamental mode. In practice, it is not clear what contribution to the lhs of equation (11) will be due to scattering of the fundamental mode; isolation of the latter effect would be of importance. It might be expected that for deep events the signal due to overtones would be dominant. Application of this procedure of mode separation should lead to better knowledge of dispersion and attenuation of overtones.

3 Tests with synthetic and actual data

The synthetic seismogram shown in Fig. 1 has been obtained by superposition of the fundamental spheroidal modes computed for a perturbed model IREM of Dziewonski & Anderson

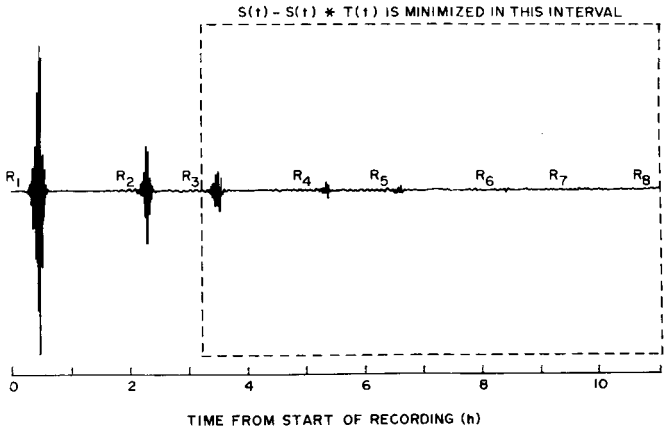

Figure 1. Synthetic seismogram for an 'unknown' structure. The seismogram contains contributions of modes from ${}_0S_2$ to ${}_0S_{97}$; source was at a depth of 70 km and receiver at a distance of 60° from the epicentre. The seismogram has been convolved with the long-period WWSSN response and a tapered low-pass filter applied to remove energy at periods shorter than 100 s. Using the technique described in this report, we shall derive elements of the elastic and anelastic earth structure consistent with information on dispersion and attenuation of surface waves contained in this recording.

Table 1. The earth model used to generate the synthetic seismogram shown in Fig. 1 was obtained by perturbing the shear velocities and attenuation of model IREM of Dziewonski & Anderson (1979) by the amounts listed in the table. The quantity q is the reciprocal of the quality factor Q.

Depth range (km)	δv_S (km s^{-1})	δq
19–80	0.1	−0.0030
80–220	−0.1	0.0025
220–400	0.1	−0.0032
400–670	−0.1	−0.0022

(1979); the amounts of perturbations are listed in Table 1. The objective of this test is to find out how our procedure will perform in determining the values of these perturbations if we use the transfer function T computed for IREM in the starting iteration. The test is a rather difficult one, as the perturbations in shear velocity offset each other; the perturbation is, roughly, zero with respect to the first two most significant eigenvalues of the inner product matrix.

The top trace in Fig. 2(a) is the 'observed' seismogram displayed for the time interval corresponding to the box in Fig. 1. The next trace is the truncated result of convolution of the complete seismogram of Fig. 1 with the transfer function computed for the starting model. Even visual inspection reveals that there are substantial differences between these two time functions. Their values are displayed in the third trace and, indeed, the amplitudes of the difference trace are comparable to those of the signal. The procedure converges despite the magnitude of initial differences, and the bottom trace shows that the residual function: $[s(t) - s(t)*T(t)]_{t_{1,2}}$ is very small and, therefore, our transfer function, obtained through waveform inversion, should represent the 'true' dispersion and attenuation rather well. The frequency domain equivalent of Fig. 2(a) is shown in Fig. 2(b), where the moduli of spectral amplitudes are displayed.

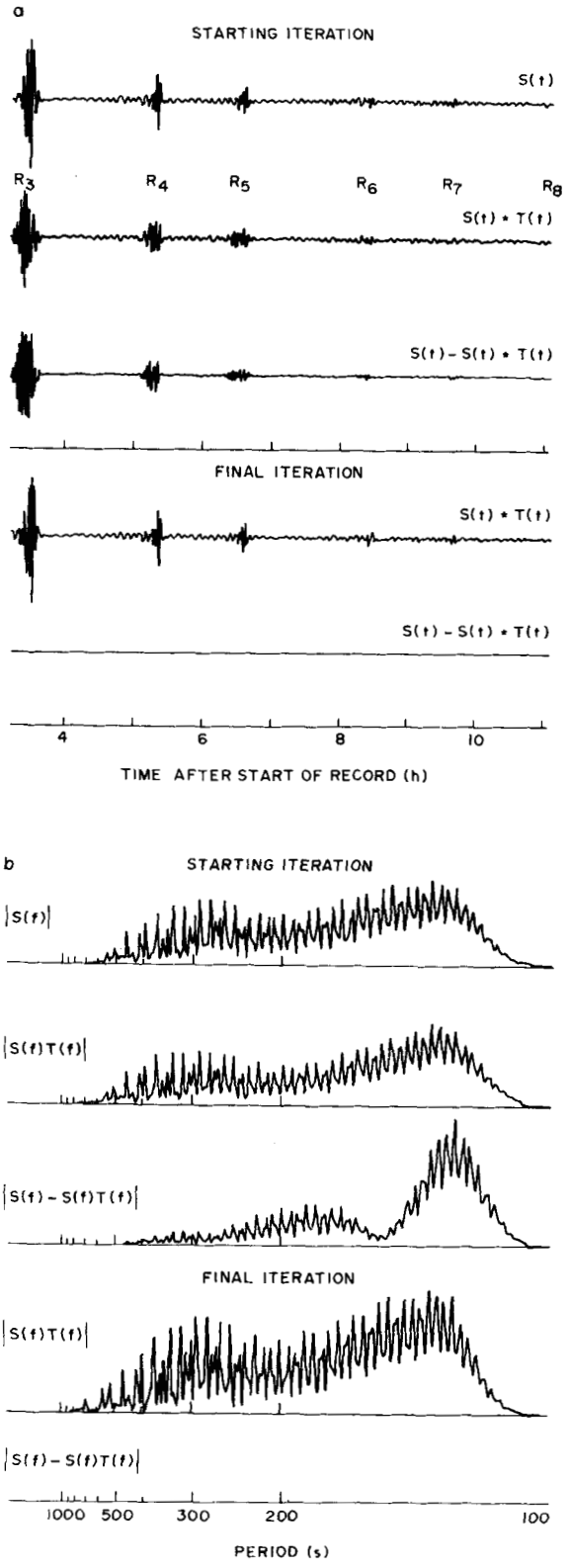

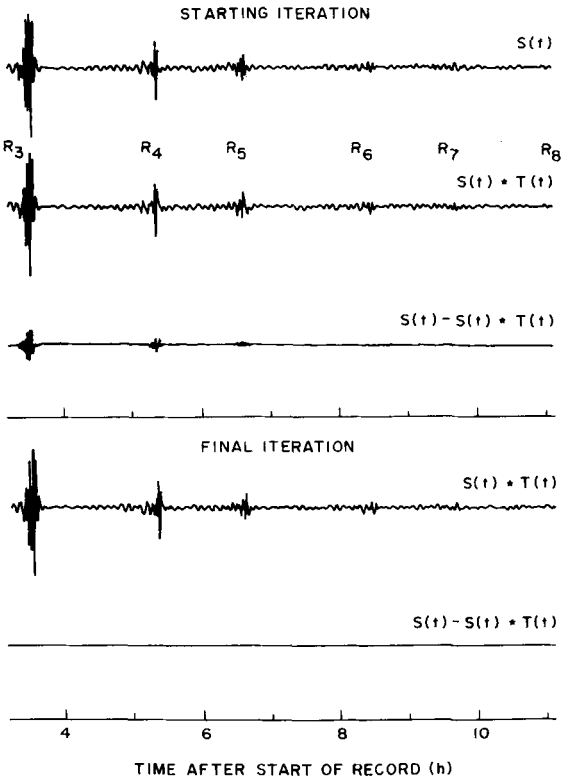

Figure 3. Same as Fig. 2(a), except for an improved starting model obtained during the first stage (pass) of inversion procedure. The discrepancy between the last trace in Fig. 2(a) and the third trace in this figure is a result of non-linear relationship between functionals of a model and perturbations in structural parameters.

Throughout all iterations that led to the final result, the differential kernels $\mathbf{G}(r, \omega)$ and group velocity $u(\omega)$ were kept unchanged, even though they are functionals of the model and the model changed during inversion. It is desirable, therefore, to recompute the eigenfrequencies and differential kernels after the first pass, and repeat the entire process. Fig. 3 demonstrates that the effect of non-linearity is discernible. The starting transfer function is now computed for the final model of 'Pass 1'. Note that amplitudes of the difference trace at the beginning of the Pass 2 are much greater than at the end of Pass 1. This means that the effect of non-linearity is important if one considers derivation of the earth model to be the principal objective of the procedure. If estimation of dispersion and attenuation is the only objective, then the accuracy of the result obtained at the end of Pass 1 will be sufficient for practical purposes.

Figure 2. (a) The top trace is the segment of the synthetic seismogram shown in Fig. 1 within the outlined area. The next trace is a truncated result of convolution of the seismogram in Fig. 1 with a transfer function T for the starting model. If the transfer function were consistent with the 'true' dispersion and attenuation, then the third trace would be zero; it clearly is not. However, in several iterations we improve the transfer function through perturbations in the model, such that the difference trace shown at the bottom of the figure is zero, for all practical purposes. (b) Frequency-domain representation of information shown in (a). Only the moduli of spectral amplitudes are shown.

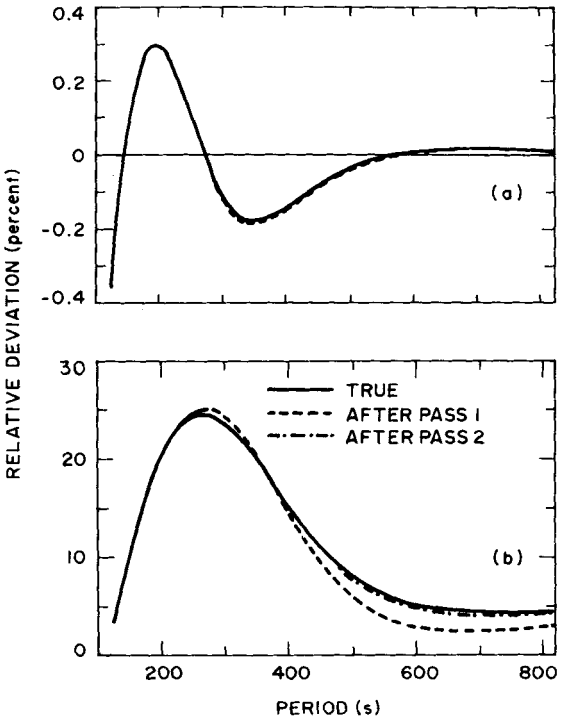

Figure 4. Comparison of (a) phase velocities and (b) attenuation obtained through the linearized inversion of waveform data with the exact results. Values for the starting model represent the reference level.

Fig. 4(a) shows comparison of the phase velocities measured after Passes 1 and 2 with the exact results; the largest difference after Pass 1 is about 5 parts in 100 000, and after Pass 2 the results agree to five significant figures. The differences in attenuation, shown in Fig. 4(b), are more substantial and for Pass 1 they reach 2 per cent at 600 s. One can expect, however, that the magnitude of this error caused by the non-linearity of the procedure is small in comparison with other sources of error that would be encountered in processing actual data.

In Fig. 5 we compare the retrieved structures with the known perturbation. The velocities after Pass 1 are very close to the correct answer – the largest deviation is 0.01 km s^{-1}, or 10 per cent of the perturbation. However, there are major differences in the Q-structure; in particular, the sign of the perturbation in the lid is opposite to the correct one. The structure derived in Pass 2 is very close to the true one. Undoubtedly, the fact that we were considering the effect of dispersion due to anelasticity throughout inversion, combined with the non-linearity of the problem led to trade-offs that primarily affect the Q-structure.

Recordings from the IDA network provide an excellent opportunity to test our method of determination of the transfer function using actual data. The response of these instruments is designed to enhance the energy at long periods, and visual examination of their records for events with magnitudes of about 7 allows one to appreciate the significant amplitudes of waves with periods greater than 300 s, seldom detectable in recordings of the WWSSN stations for events with magnitudes much less than 8.

Fig. 6 shows a recording of an event in the Solomon Islands region (1977 29 July; M_S = 7.2, NEIS) obtained at Halifax, Nova Scotia. The original recording has been processed with a tapered low-pass filter of a cut-off period of 150 s. The first wavegroup identified in this figure is R_3; the amplitudes of R_1 and R_2 exceeded the range of linearity of the instrument.

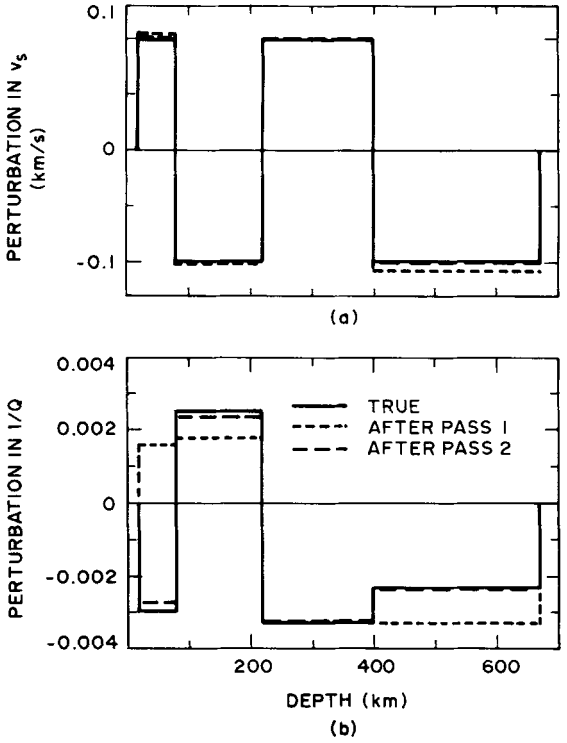

Figure 5. Comparison with the exact results of (a) shear velocity and (b) shear attenuation profiles obtained through the linearized inversion of waveform data. The starting structure represents the reference level.

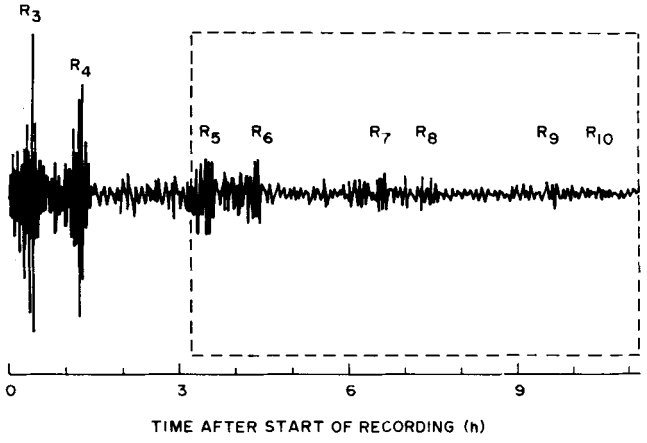

Figure 6. Recording of a Solomon Islands earthquake of 1977 July 29 by an IDA instrument at Halifax, Nova Scotia. The difference $s(t) - s(t) * T(t)$ is minimized within the area outlined by a box. Symbols R_n denote the individual arrivals of the wavegroups of mantle Rayleigh waves.

This recording probably would not have been used in the analysis of dispersion and attenuation using the standard methods, as the closeness of the arrivals R_3 and R_4 ($\Delta \sim 130^\circ$) makes the necessary separation of those and subsequent wavegroups very difficult. This figure is equivalent to Fig. 1, with the difference that the time series does not begin at the origin time.

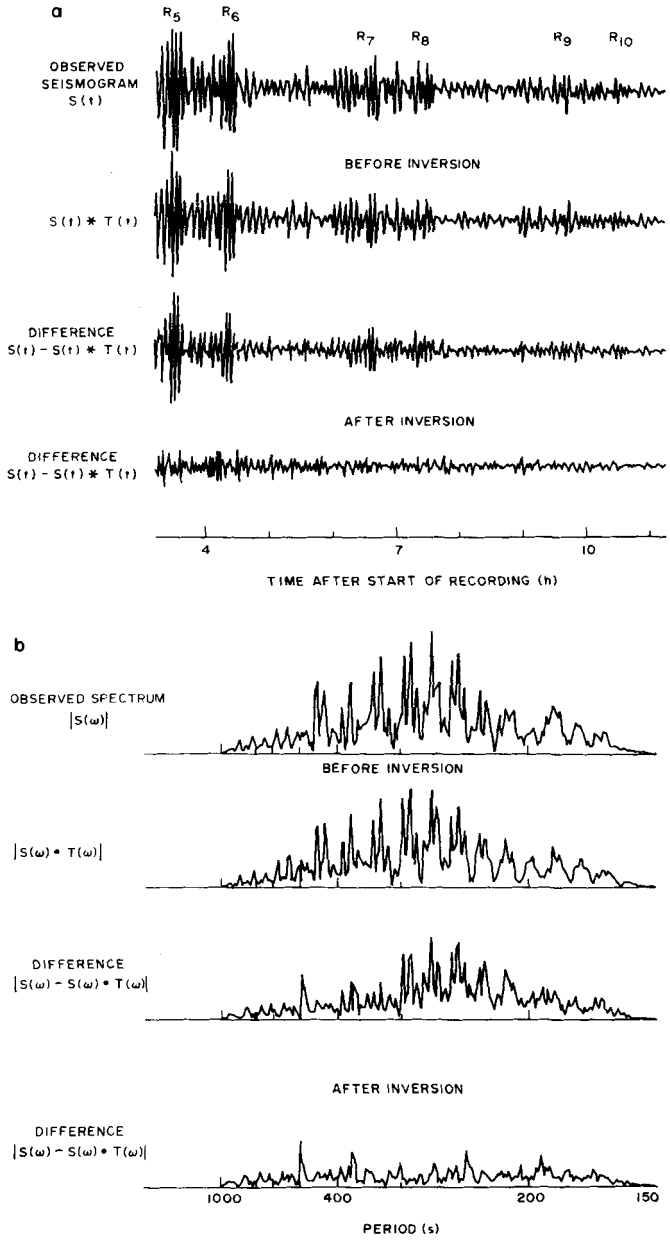

Figure 7. (a) Same as Fig. 2(a), but applied to actual data: the seismogram shown in Fig. 6. The difference trace after inversion does not show correlation with arrivals of individual wavegroups. (b) Frequency domain representation of (a); only power spectra are shown. The spectrum of the difference trace after inversion appears to be white and that there is no correlation with spectral peaks of the fundamental spheroidal mode.

The difference trace in Fig. 7(a) shows that the transfer function for the reference model (IREM) deviates perceptibly from that appropriate for this path. There is clear correlation between the large amplitudes of the difference trace and the occurrence of the wavegroups in the observed seismogram. However, after inversion, the envelope of the difference signal

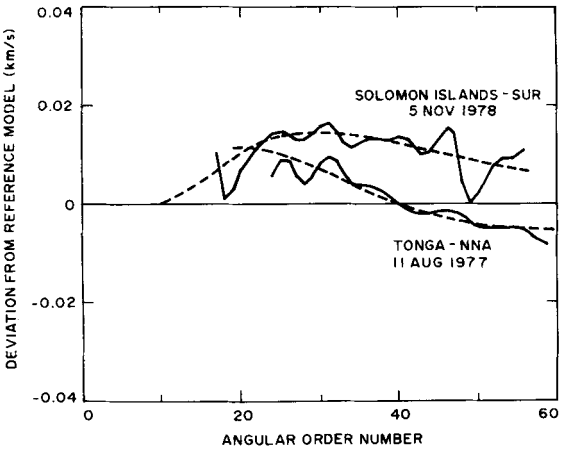

Figure 8. Comparison of phase velocities obtained by the waveform inversion technique (WIT; broken lines), described in this report, with those measured using the traditional phase-delay method (solid lines). Curves obtained by application of WIT are naturally smooth and can easily be differentiated to obtain group velocities, for example.

decreases smoothly with time; this gradual decrease in the frequency content suggests that it represents an attenuated seismic signal associated with the overtones and scattered energy of the fundamental mode.

The equivalent trace in Fig. 7(b), representing the power spectrum of the residual trace, indicates no correlation with the spectral peaks of the fundamental spheroidal mode, and that the overall character of this trace is white (in order to recover spectral peaks of the overtones, the operation implied by equation (11) of the previous section must be performed).

The purpose of Fig. 8 is to demonstrate that dispersion measured using WIT is in general agreement with the results obtained by application of standard techniques. The continuous lines in that figure represent results of phase velocity measurements using the approach of Dziewonski & Landisman (1970), in which the phase delay function is obtained from the analysis of the appropriately selected fragment of the auto-correlogram of the observed seismogram; the broken lines are the values resulting from application of WIT. It is clear that there is an overall correspondence between these two sets of answers; the smooth lines represent the trend of the results from the phase delay analysis, but in addition to being physically realistic, they also extend to substantially longer periods. It is also clear that for different paths the trends in the data can be different at periods longer than 300 s.

Fig. 9 demonstrates the repeatability of the results. Two strong earthquakes in the Solomon Islands (M_S 6.9 and 7.3; NEIS) occurred within 22 hr of each other; their locations were very close, and visual inspection of several recordings indicates that their source mechanisms were also similar. The two dispersion curves are practically identical within a large range of angular order numbers (from 9 to 55, corresponding to a period range from 630 to 165 s) and the maximum difference at short periods is about 0.03 per cent. This agreement is even more remarkable, as the delay of the analysis with respect to the origin time was different for the two recordings because of the disparity in their magnitude.

In summary, the method appears to be highly stable and yields repeatable results. Information obtained through the experiment with synthetic data indicates that if the only objective of application of WIT is to estimate the dispersion and attenuation for a particular path, then it is sufficient to perturb the starting model through a series of iterations.

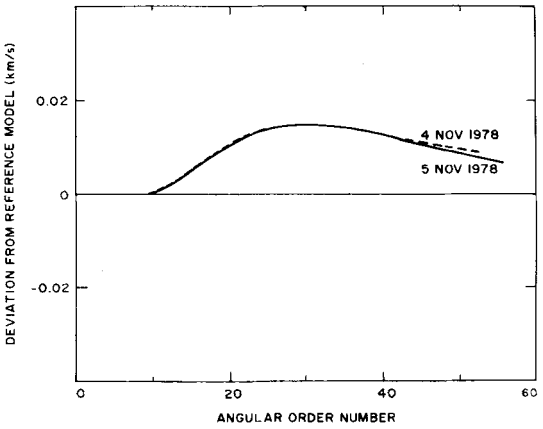

Figure 9. Repeatability of measurements is demonstrated by results of the analyses of two recordings at Sutherland, South Africa of earthquakes of nearly identical location and similar source mechanism.

However, if the recovery of structure is important, then the functionals such as the periods of normal modes, group velocities and Q, as well as the appropriate differential kernels should be recalculated through the solution of differential equations and the inversion procedure repeated. This, of course, requires much more computation.

4 Derivation of 'pure path' dispersion and attenuation using the geometrical ray theory approximation

Numerous analyses based on geometrical ray theory have been performed in the past (Toksöz & Anderson 1966; Kanamori 1970; Dziewonski 1971; Wu 1972; Nakanishi 1979, 1981; Lévêque 1980; Silver & Jordan 1981). The results obtained in these studies have been used to infer the depth to which lateral variations in the elastic and anelastic parameters are correlated with the surficial tectonic nature of a given region. Implications of these inferences can be of fundamental importance to our understanding the dynamics of the mantle. The results presented in this section might be understood as a test of WIT in application to this type of analysis. Also, there is an indication that extension of measurements to 600 s provides important structural constraints.

The basis of the 'pure path' method was originally an assumption that the elastic parameters underneath the regions of the same tectonic type (for example, shields or young oceanic floor) are identical. This assumption was justified by the observed similarity of short period (30–100 s) dispersion curves measured for the regions of analogous tectonic nature in different parts of the world (for a review, see Knopoff 1972).

If the set of observations is large (many intersecting paths) in comparison with the number of hypothetical regions, the meaning of the 'pure path' analysis may be perceived differently. The structures within a given type of region need not be identical; we determine the average structure for each region. The error analysis should reveal whether the differences are statistically significant. Different regionalization schemes may be tested in this way; regionalization may also be depth dependent, although we do not explore this option here.

Thus the Earth's surface is divided into several types, N, of tectonic regions. For a jth great circle path of a given data set, the difference between the observed and reference frequency of a given mode is:

$$\delta\omega_j = \sum_{i=1}^{N} p_{ij}\delta\omega_i; \qquad (12)$$

where p_{ij} is the fractional path length for the ith region type and the jth path; the fractional path lengths are obtained by line integration along the great circle path. This procedure was first proposed by Toksöz & Anderson (1966), and has been used only with minor changes in all 'pure path' studies so far.

The fractional path lengths defined in this way do not depend on the angular order (wavelength) or on the specific position of the source and receiver, as long as they lie on the same great circle. Having a sufficient number of observations, the equations of condition (12) can be reduced to a system of normal equations using the least squares measure and then solved for the 'pure path' or 'local' eigenfrequency.

Woodhouse & Girnius (1982) showed that the appropriate expression for the eigenfrequency observed for the jth source-receiver pair has the form:

$$\delta\omega_j = \sum_{m=0}^{2} \sum_{i=1}^{N} p_{ij}^{(m)} \cdot \delta\omega_i^{(m)} . \tag{13}$$

There are, thus, three types of local eigenfrequencies and corresponding fractional path lengths; each type of local eigenfrequency is related to the local structure through a different set of differential kernels. (For this reason, the philosophy of WIT, in which the inversion is made for the structural parameters of a model without direct determination of its functionals, such as eigenfrequencies, seems to be ideally suited for application of the theory of Woodhouse & Girnius.) Numerical experiments performed by those authors show that distortions are the most severe for regions small in their overall area and irregular in shape.

It is clear that in the future the advanced theory must be used to interpret observations correctly. Yet, equation (12) can lead to useful results at a certain level of application. The 'pure path' structures obtained using WIT can be used to represent starting transfer functions for arbitrary paths, thus reducing the initial level of discrepancy between the data and prediction. The synthetic transfer functions could be used to reduce the effect of lateral heterogeneity in inversion for the seismic moment tensor. Also, we consider the application described in this section as an important test of the method itself.

From a large number of visually examined seismograms and their spectra we have selected 37 recordings that showed the best signal-to-noise ratio. The great circle paths and their poles are shown in Fig. 10. The poles have a fairly uniform distribution in longitude, but nearly-equatorial latitudes (corresponding to nearly polar paths) are poorly represented. In the future particular effort should be made to assure good geographical coverage.

The surface of the Earth is well sampled by the great circle paths, particularly if one considers distortion of the area by the linear projection of geographic coordinates. The North Atlantic, northern Eurasia and their antipodes are the only regions that are seriously undersampled. However, if anisotropy should represent an important factor, then each region should be sampled by paths traversing it at different azimuths. Most of the paths sampling the Indian Ocean, for example, are nearly parallel.

The matching of transfer functions for individual paths was achieved by perturbation of three parameters in shear velocity (constant perturbations in the depth ranges: 80–220, 220–400 and 400–670 km) and two in Q (perturbations in depth ranges from 80 to 400 km and from 400 to 670 km). The experiments discussed in the previous section demonstrate that variation of these parameters is sufficient to obtain good transfer functions. Clearly, other representations, including transverse anisotropy (Dziewonski & Anderson 1981), are feasible. The range of frequencies (angular order numbers) used in inversion was determined through visual examination of the spectra: the total span of the order numbers used is from 7 to 60 (from 800 to 150 s, roughly) but it varied appreciably from record to record. For

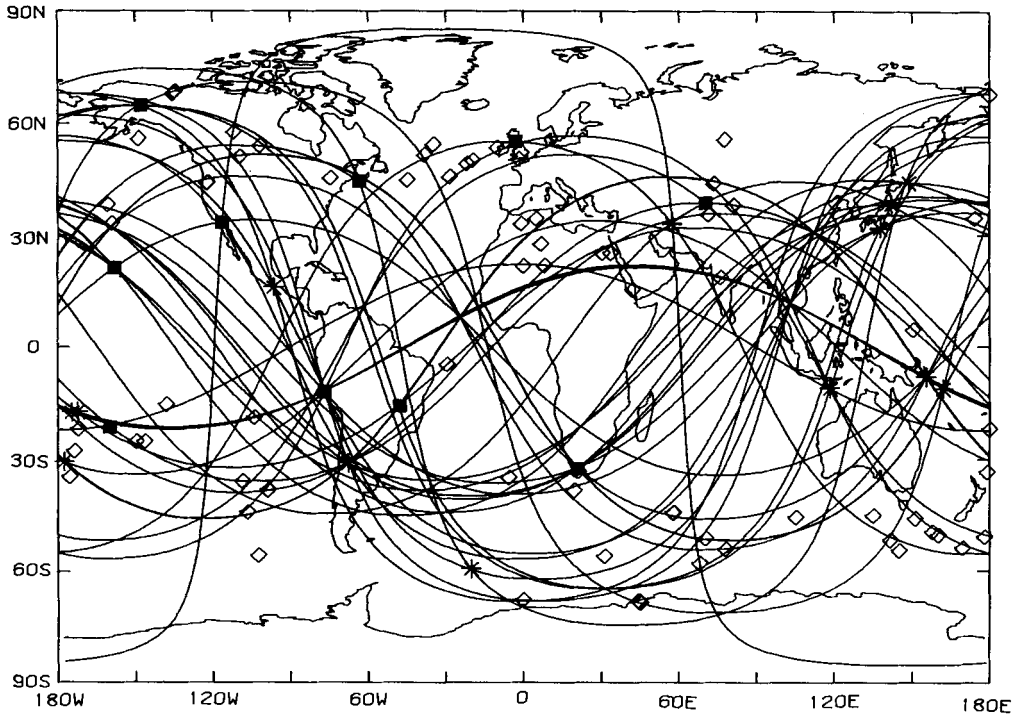

Figure 10. Great circle paths and their poles (diamonds) for 37 recordings analysed in this study. Filled squares are IDA stations and stars are the sources.

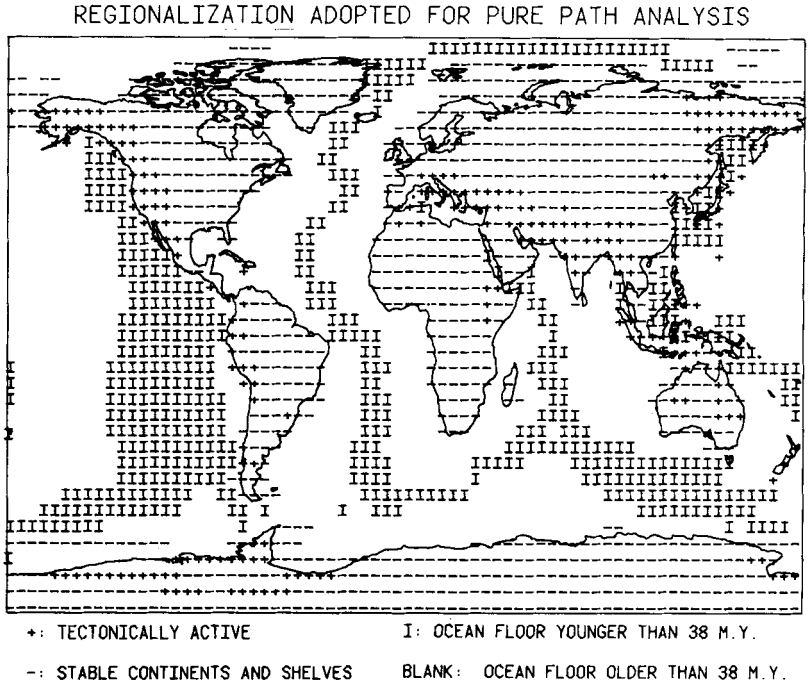

Figure 11. Schematic representation of regionalization adopted in our 'pure path' analysis. This regionalization has been obtained by combining several regions of similar tectonic nature as defined by Mauk (1977). The projection is the same as in Fig. 10.

this reason, one should not anticipate full correspondence between the results of regionalization using the model or data space.

The regionalization adopted here is based on the work of Mauk (1977), who divided the world into 20 types of regions, using a $5° \times 5°$ grid and considered fractional contributions (with a precision of one tenth) of individual regions to a given cell. We have combined Mauk's regions into four types: (1) stable continents, including continental shelves, for which tectonic activity ceased at least 400 Myr ago; (2) tectonic, including island arcs; (3) ocean floors younger than 38 Myr; and (4) ocean floors older than 38 Myr. Perhaps a more detailed regionalization will be warranted in the future, when the number of paths increases significantly. Fig. 11 is a map of the world schematically showing our regionalization. Fractional contributions for each cell were considered in actual calculation of path compositions. The projection is the same as in Fig. 10.

After the data obtained through application of WIT to individual paths were corrected for ellipticity (Dahlen 1975; Dziewonski & Sailor 1976), the 'pure path' decomposition was calculated for the system of equations of condition (12). The results for periods of normal modes, group velocities and Q are presented in Table 2 for the range of angular order numbers from 9 to 55. The differences of 'pure path' phase and group velocities from those computed for PREM (Preliminary Reference Earth Model; Dziewonski & Anderson 1981) are shown in Fig. 12(a, b). Roughness of the curves at frequencies lower than 3 mHz and, in particular, higher than 5 mHz is the result of the fact that data were not available for all the paths outside the 3–5 mHz range. Except for roughness, there is no overall change in the trend due to variations in the path coverage; this indicates the stability of the inverse problem.

Table 2. Results of 'pure path' analysis for periods of normal modes, their group velocities and attenuation for the four regions defined in Fig. 11 using the data from 37 great circle paths which, together with their poles, are shown in Fig. 10. The column 'MODE' gives the angular order number l of the fundamental mode series ${}_0S_l$.

	NORMAL MODE PERIODS								GROUP VELOCITY								ATTENUATION							
MODE	STABLE CONT		TECTONIC		YOUNG OCEAN		OLD OCEAN		STABLE CONT		TECTONIC		YOUNG OCEAN		OLD OCEAN		STABLE CONT		TECTONIC		YOUNG OCEAN		OLD OCEAN	
	PERIOD	S.D.	PERIOD	S.D.	PERIOD	S.D.	PERIOD	S.D.	GR VEL	S.D.	GR VEL	S.D.	GR VEL	S.D.	GR VEL	S.D.	Q	S.D.	Q	S.D.	Q	S.D.	Q	S.D.
	s		s		s		s		s		s		s		s									
9	633.62	0.05	634.22	0.09	634.24	0.06	633.66	0.03	6.228	0.19	6.247	0.38	6.242	0.24	6.253	0.11	319.6	8.4	395.4	20.9	327.9	10.9	319.5	5.1
10	579.32	0.04	579.56	0.06	579.78	0.05	579.31	0.02	5.641	0.15	5.665	0.22	5.649	0.16	5.664	0.07	318.5	7.1	359.3	12.0	341.4	8.4	301.3	3.0
11	537.21	0.05	537.30	0.07	537.44	0.05	536.89	0.02	5.240	0.19	5.262	0.27	5.242	0.21	5.272	0.08	321.3	7.7	325.7	11.1	321.0	8.4	304.9	3.1
12	502.77	0.06	502.67	0.08	502.97	0.06	502.26	0.02	4.982	0.22	5.009	0.31	4.982	0.23	5.023	0.09	317.7	7.6	314.9	10.5	314.0	8.0	297.2	3.0
13	473.67	0.06	473.45	0.09	473.90	0.07	472.99	0.03	4.801	0.25	4.826	0.36	4.790	0.27	4.846	0.11	309.6	7.6	310.8	11.0	307.3	8.1	290.6	3.1
14	448.46	0.06	448.22	0.10	448.98	0.07	447.71	0.03	4.660	0.23	4.678	0.39	4.627	0.27	4.704	0.12	308.7	7.0	303.1	11.2	290.7	7.4	284.0	3.2
15	426.49	0.07	426.20	0.11	427.14	0.08	425.61	0.04	4.532	0.26	4.545	0.43	4.489	0.30	4.578	0.13	304.7	8.0	295.1	12.7	278.0	8.2	275.2	3.6
16	407.08	0.07	406.77	0.13	407.87	0.09	406.09	0.04	4.415	0.27	4.420	0.45	4.360	0.31	4.461	0.14	300.1	9.2	286.6	14.5	265.3	9.2	265.9	4.1
17	389.79	0.08	389.49	0.14	390.72	0.09	388.70	0.04	4.305	0.28	4.306	0.47	4.244	0.33	4.351	0.15	294.8	10.7	277.9	16.6	253.0	10.3	256.5	4.6
18	374.27	0.09	374.01	0.15	375.37	0.10	373.12	0.05	4.204	0.29	4.198	0.48	4.134	0.34	4.246	0.15	288.9	12.2	269.0	18.6	241.3	11.4	247.0	5.2
19	360.21	0.10	360.11	0.16	361.40	0.11	359.12	0.05	4.113	0.28	4.095	0.48	4.038	0.33	4.150	0.15	283.8	13.4	259.3	20.2	232.7	12.2	236.4	5.4
20	347.47	0.10	347.44	0.17	348.82	0.11	346.34	0.05	4.034	0.29	4.001	0.48	3.945	0.33	4.063	0.15	277.1	14.7	250.9	21.9	222.6	13.0	227.6	5.8
21	335.81	0.10	335.88	0.17	337.32	0.12	334.68	0.05	3.958	0.30	3.918	0.51	3.865	0.35	3.986	0.15	270.2	15.8	242.8	23.4	213.6	13.8	219.1	6.2
22	325.09	0.11	325.27	0.18	326.76	0.12	323.98	0.05	3.895	0.32	3.841	0.54	3.796	0.37	3.917	0.16	263.2	16.7	235.2	24.5	205.5	14.4	211.2	6.5
23	315.18	0.11	315.49	0.18	317.00	0.12	314.10	0.06	3.842	0.31	3.779	0.53	3.734	0.36	3.855	0.16	256.2	17.4	228.0	25.5	198.3	14.9	203.9	6.7
24	305.98	0.11	306.42	0.18	307.94	0.12	304.93	0.06	3.796	0.31	3.726	0.53	3.688	0.36	3.799	0.16	249.3	18.0	221.3	26.3	191.9	15.3	197.1	6.9
25	297.39	0.11	297.96	0.18	299.48	0.12	296.40	0.06	3.758	0.33	3.677	0.57	3.646	0.39	3.754	0.17	242.6	18.3	215.0	26.7	186.3	15.6	190.8	7.0
26	289.34	0.11	290.06	0.19	291.56	0.13	288.41	0.06	3.726	0.34	3.638	0.59	3.610	0.40	3.717	0.18	236.0	18.5	209.3	27.0	181.4	15.7	185.1	7.1
27	281.77	0.11	282.64	0.19	284.11	0.13	280.91	0.06	3.700	0.36	3.607	0.63	3.583	0.43	3.686	0.19	229.7	18.6	204.0	27.1	177.1	15.9	179.8	7.1
28	274.64	0.11	275.64	0.19	277.09	0.13	273.85	0.06	3.681	0.38	3.572	0.66	3.557	0.44	3.660	0.20	223.6	18.6	199.0	27.3	173.3	15.9	174.9	7.1
29	267.88	0.11	269.04	0.19	270.44	0.13	267.17	0.06	3.663	0.38	3.555	0.66	3.541	0.45	3.638	0.20	217.8	18.5	194.5	27.2	170.0	16.0	170.4	7.0
30	261.48	0.12	262.77	0.19	264.13	0.13	260.85	0.06	3.653	0.38	3.534	0.66	3.525	0.45	3.624	0.20	212.2	18.3	190.3	27.0	167.1	16.0	166.3	7.0
31	255.39	0.12	256.82	0.20	258.13	0.13	254.84	0.06	3.644	0.38	3.517	0.67	3.512	0.45	3.612	0.20	206.9	18.1	186.4	26.8	164.6	15.9	162.4	6.9
32	249.59	0.12	251.16	0.20	252.41	0.13	249.11	0.06	3.638	0.38	3.507	0.65	3.505	0.44	3.602	0.20	201.9	17.9	182.8	26.7	162.5	15.9	158.9	6.8
33	244.05	0.12	245.75	0.20	246.95	0.14	243.65	0.06	3.635	0.39	3.499	0.67	3.500	0.45	3.596	0.20	197.1	17.6	179.4	26.4	160.6	15.9	155.6	6.8
34	238.76	0.12	240.59	0.21	241.73	0.14	238.43	0.06	3.634	0.38	3.490	0.66	3.495	0.45	3.593	0.20	192.5	17.4	176.3	26.3	159.0	15.9	152.6	6.7
35	233.69	0.13	235.64	0.21	236.73	0.14	233.44	0.07	3.634	0.39	3.486	0.68	3.494	0.46	3.591	0.20	188.2	17.2	173.4	26.2	157.7	15.9	149.7	6.6
36	228.83	0.13	230.91	0.21	231.93	0.14	228.65	0.07	3.636	0.39	3.482	0.69	3.489	0.46	3.593	0.21	184.0	17.0	170.7	25.9	156.5	16.0	147.1	6.6
37	224.16	0.13	226.36	0.22	227.33	0.15	224.05	0.07	3.639	0.40	3.480	0.71	3.491	0.48	3.592	0.21	180.1	16.9	168.2	25.9	155.6	16.2	144.6	6.6
38	219.68	0.14	221.98	0.22	222.91	0.15	219.63	0.07	3.642	0.42	3.479	0.74	3.492	0.50	3.595	0.22	176.4	16.8	165.8	26.0	154.9	16.3	142.2	6.6
39	215.38	0.14	217.78	0.23	218.65	0.15	215.37	0.07	3.646	0.43	3.479	0.76	3.493	0.51	3.600	0.23	172.8	16.7	163.6	26.2	154.3	16.5	140.0	6.6
40	211.26	0.15	213.71	0.24	214.56	0.16	211.26	0.08	3.646	0.46	3.483	0.80	3.491	0.54	3.607	0.24	170.1	17.4	161.1	26.7	153.9	17.1	137.8	6.8
41	207.26	0.15	209.80	0.24	210.62	0.16	207.31	0.08	3.648	0.49	3.485	0.85	3.494	0.58	3.614	0.26	166.9	17.5	159.1	27.1	153.6	17.5	135.8	6.9
42	203.42	0.15	206.03	0.25	206.81	0.17	203.50	0.08	3.651	0.53	3.489	0.92	3.498	0.62	3.620	0.28	163.9	17.7	157.3	27.5	153.4	18.0	134.0	7.0
43	199.71	0.16	202.39	0.26	203.13	0.17	199.81	0.08	3.657	0.59	3.494	1.01	3.498	0.68	3.627	0.31	161.0	17.9	155.5	28.0	153.4	18.4	132.2	7.1
44	196.12	0.16	198.87	0.26	199.59	0.18	196.26	0.08	3.662	0.63	3.498	1.09	3.500	0.73	3.633	0.33	158.2	18.0	153.9	28.5	153.4	19.0	130.5	7.2
45	192.69	0.17	195.45	0.28	196.17	0.19	192.80	0.09	3.663	0.71	3.503	1.20	3.503	0.81	3.642	0.37	159.4	19.3	149.2	28.9	154.8	20.0	127.9	7.4
46	189.30	0.17	192.27	0.28	192.81	0.19	189.48	0.09	3.672	0.74	3.496	1.27	3.507	0.85	3.650	0.38	158.1	20.1	145.5	29.8	155.9	21.2	126.3	7.7
47	186.09	0.18	189.18	0.28	189.51	0.19	186.29	0.09	3.676	0.81	3.497	1.40	3.514	0.98	3.657	0.42	157.0	20.7	149.2	31.8	151.2	21.6	126.0	8.0
48	182.93	0.18	186.05	0.29	186.46	0.20	183.19	0.09	3.684	0.86	3.505	1.48	3.513	1.00	3.662	0.45	150.6	20.0	143.5	30.9	157.9	22.9	126.2	8.1
49	179.89	0.19	183.06	0.30	183.45	0.21	180.16	0.10	3.690	0.93	3.510	1.60	3.513	1.08	3.671	0.48	148.2	20.5	142.3	31.6	158.6	23.6	125.1	8.3
50	176.97	0.20	180.12	0.33	180.50	0.22	177.26	0.11	3.691	0.98	3.529	1.71	3.526	1.16	3.668	0.53	146.8	20.6	152.5	35.1	156.9	24.2	120.7	8.6
51	173.96	0.22	177.53	0.36	177.81	0.24	174.41	0.11	3.710	1.11	3.512	1.92	3.515	1.29	3.678	0.57	144.6	21.1	151.1	36.0	157.8	25.1	119.7	8.8
52	171.30	0.23	174.62	0.39	174.95	0.25	171.71	0.12	3.697	1.02	3.540	1.87	3.542	1.21	3.674	0.53	136.4	20.7	159.9	42.7	169.7	29.4	116.2	9.1
53	168.63	0.23	171.96	0.40	172.28	0.26	169.05	0.12	3.701	1.07	3.542	1.96	3.541	1.27	3.680	0.55	134.2	21.1	160.9	44.4	170.4	30.5	115.4	9.3
54	165.87	0.26	168.95	0.44	170.05	0.31	166.43	0.13	3.725	1.20	3.580	2.21	3.517	1.56	3.690	0.64	147.8	25.7	155.9	48.0	151.2	32.2	117.2	10.7
55	163.35	0.27	166.43	0.46	167.54	0.32	163.91	0.14	3.730	1.26	3.583	2.31	3.518	1.63	3.698	0.67	145.9	26.3	156.2	49.7	151.6	33.4	116.5	11.0

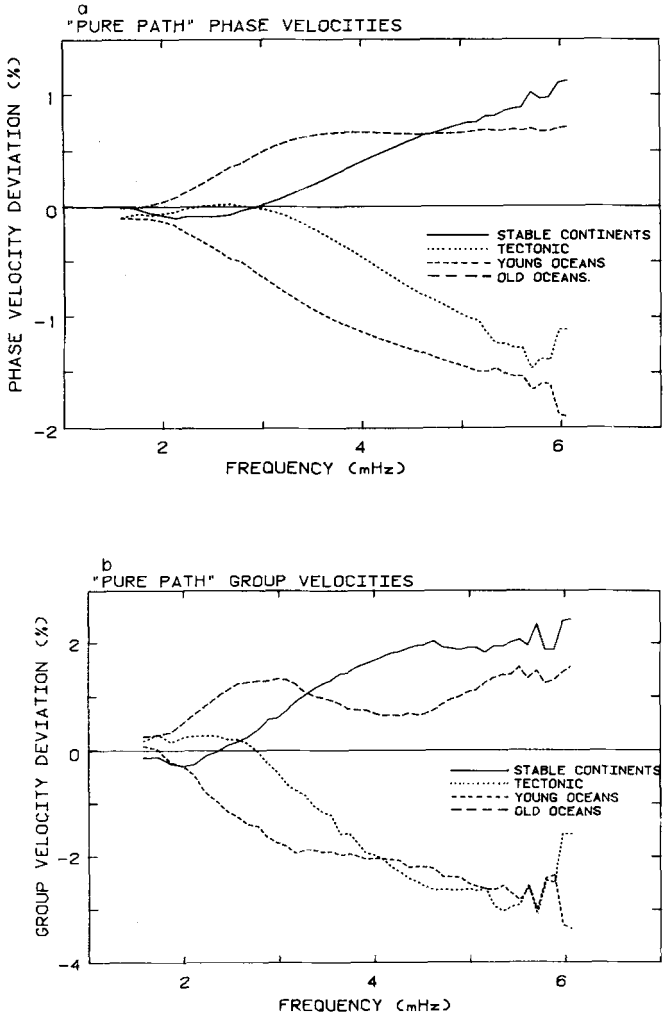

Figure 12. (a) 'Pure path' phase velocities obtained through decomposition of the results of measurements for 37 great circle paths. Roughness, particularly noticeable at the high-frequency end, results from the fact that the range of order numbers varied for individual recordings, and at the low- and high-frequency ends the answers were obtained from substantially fewer than 37 values. The fact that the overall trend remains the same seems to be indicative of the stability of our data set and regionalization scheme. (b) Same as (a) but for 'pure path' group velocities.

At frequencies higher than 4 mHz (250 s), the major differences are between young oceans and tectonic regions on one hand and stable continents and old oceans on the other. This is qualitatively consistent with the results of previous studies of this kind. Phase velocities become very close to each other at the lower frequency range of analysis (1.57 mHz), but then begin to diverge in a rather distinct manner: for the stable continents and tectonic regions the phase velocities follow the global average and are very close to each other up to a 3 mHz frequency, while the values for old and young oceans begin to diverge much earlier. A similar trend can be inferred from the results of Silver & Jordan (1981) for the end members of their regionalization of continental and oceanic areas. An intuitive interpretation would imply deep seated differences in structure underneath the young and old oceans.

Table 3. Comparison of periods of normal modes, their group velocities and attenuation with the properly weighted average of all data and the appropriate functionals computed for model PREM of Dziewonski & Anderson (1981). Notice that the differences between the continental and oceanic attenuation are statistically significant, except at the high-frequency end of the analysis.

	NORMAL MODE PERIODS				GROUP VELOCITY				ATTENUATION							
MODE	CONTINENT PERIOD S.D.		OCEAN PERIOD S.D.		AVERAGE PERIOD S.D.		PREM PERIOD	CONTINENT GR VEL S.D.		OCEAN GR VEL S.D.		AVERAGE GR VEL S.D.		PREM GR VEL	CONTINENT Q S.D.		OCEAN Q S.D.		AVERAGE Q S.D.		PREM Q
		%		%		%			%		%		%			%		%		
9	633.86	0.02	633.83	0.01	633.84	0.00	633.61	6.232	0.09	6.249	0.06	6.243	0.02	6.237	338.9	4.4	321.2	2.5	327.6	0.7	332.7
10	579.49	0.02	579.42	0.01	579.45	0.00	579.22	5.646	0.07	5.659	0.05	5.654	0.01	5.648	339.4	3.5	309.5	2.0	320.2	0.6	327.8
11	537.35	0.02	537.03	0.01	537.15	0.00	536.94	5.242	0.10	5.263	0.06	5.255	0.02	5.254	326.1	3.4	308.7	2.0	314.9	0.6	322.1
12	502.86	0.03	502.45	0.02	502.60	0.00	502.42	4.985	0.12	5.011	0.07	5.001	0.02	4.997	319.9	3.3	301.5	1.9	308.1	0.5	315.2
13	473.75	0.03	473.24	0.02	473.43	0.01	473.28	4.800	0.14	4.830	0.08	4.819	0.02	4.813	313.1	3.4	294.8	1.9	301.3	0.5	307.2
14	448.55	0.04	448.09	0.02	448.26	0.01	448.15	4.656	0.16	4.681	0.10	4.672	0.03	4.665	307.9	3.4	286.0	1.9	293.7	0.6	298.3
15	426.60	0.04	426.06	0.02	426.26	0.01	426.19	4.524	0.18	4.552	0.11	4.542	0.03	4.533	301.9	3.8	276.2	2.1	285.2	0.6	288.8
16	407.21	0.05	406.61	0.03	406.83	0.01	406.80	4.403	0.20	4.432	0.12	4.421	0.04	4.411	295.4	4.4	266.1	2.4	276.2	0.7	278.9
17	389.96	0.05	389.29	0.03	389.54	0.01	389.55	4.291	0.21	4.321	0.13	4.310	0.04	4.298	288.4	5.1	255.9	2.7	267.0	0.8	268.9
18	374.49	0.06	373.77	0.04	374.03	0.01	374.07	4.187	0.22	4.214	0.13	4.204	0.04	4.193	281.1	5.8	245.8	3.0	257.7	0.9	259.1
19	360.51	0.06	359.77	0.04	360.04	0.01	360.11	4.091	0.22	4.119	0.13	4.109	0.04	4.097	274.6	6.3	235.9	3.3	248.9	1.0	249.7
20	347.82	0.07	347.04	0.04	347.33	0.01	347.42	4.006	0.23	4.031	0.14	4.021	0.04	4.011	267.0	6.8	226.7	3.5	240.1	1.1	240.8
21	336.22	0.07	335.43	0.04	335.72	0.01	335.83	3.927	0.24	3.953	0.15	3.944	0.04	3.934	259.5	7.3	218.1	3.7	231.8	1.1	232.4
22	325.56	0.08	324.76	0.05	325.06	0.01	325.18	3.860	0.25	3.884	0.15	3.875	0.04	3.866	252.2	7.7	210.2	3.9	224.0	1.2	224.8
23	315.71	0.08	314.91	0.05	315.20	0.01	315.33	3.804	0.25	3.823	0.15	3.816	0.04	3.808	245.1	8.0	202.9	4.0	216.7	1.2	217.7
24	306.56	0.08	305.77	0.05	306.06	0.01	306.20	3.757	0.24	3.770	0.15	3.765	0.04	3.758	238.3	8.3	196.2	4.1	209.9	1.3	211.3
25	298.03	0.08	297.25	0.05	297.54	0.02	297.68	3.716	0.25	3.726	0.15	3.722	0.04	3.716	231.9	8.4	190.1	4.2	203.7	1.3	205.4
26	290.04	0.09	289.28	0.05	289.56	0.02	289.70	3.682	0.25	3.690	0.15	3.687	0.04	3.681	225.8	8.5	184.5	4.2	197.9	1.3	200.0
27	282.53	0.09	281.79	0.05	282.06	0.02	282.20	3.654	0.26	3.660	0.16	3.658	0.04	3.652	220.0	8.6	179.5	4.2	192.7	1.3	195.1
28	275.44	0.09	274.73	0.06	274.99	0.02	275.13	3.630	0.27	3.635	0.16	3.633	0.04	3.629	214.7	8.6	174.9	4.2	187.8	1.3	190.7
29	268.74	0.09	268.06	0.06	268.31	0.02	268.44	3.613	0.26	3.614	0.16	3.614	0.04	3.611	209.6	8.6	170.7	4.2	183.3	1.3	186.6
30	262.39	0.10	261.73	0.06	261.97	0.02	262.09	3.600	0.27	3.600	0.16	3.600	0.05	3.597	204.8	8.5	166.9	4.2	179.2	1.3	182.9
31	256.34	0.10	255.72	0.06	255.95	0.02	256.06	3.588	0.27	3.588	0.16	3.588	0.05	3.586	200.3	8.5	163.4	4.2	175.4	1.3	179.5
32	250.59	0.10	249.99	0.06	250.21	0.02	250.32	3.581	0.27	3.579	0.16	3.580	0.04	3.578	196.1	8.4	160.2	4.1	171.9	1.3	176.4
33	245.09	0.10	244.53	0.06	244.74	0.02	244.83	3.577	0.27	3.573	0.17	3.574	0.05	3.573	192.1	8.3	157.3	4.1	168.6	1.3	173.4
34	239.84	0.10	239.30	0.06	239.50	0.02	239.59	3.573	0.28	3.569	0.17	3.571	0.05	3.569	188.4	8.2	154.6	4.1	165.6	1.3	170.7
35	234.81	0.11	234.30	0.06	234.49	0.02	234.57	3.572	0.28	3.568	0.17	3.569	0.05	3.568	184.9	8.2	152.1	4.1	162.8	1.3	168.2
36	229.99	0.11	229.51	0.07	229.69	0.02	229.76	3.570	0.29	3.568	0.18	3.569	0.05	3.568	181.5	8.1	149.8	4.0	160.2	1.2	165.9
37	225.36	0.11	224.90	0.07	225.08	0.02	225.14	3.572	0.30	3.568	0.18	3.570	0.05	3.569	178.4	8.1	147.7	4.0	157.8	1.2	163.6
38	220.92	0.11	220.48	0.07	220.64	0.02	220.70	3.574	0.31	3.571	0.19	3.572	0.05	3.571	175.5	8.1	145.7	4.1	155.5	1.2	161.6
39	216.64	0.12	216.22	0.07	216.38	0.02	216.43	3.576	0.32	3.574	0.19	3.575	0.05	3.573	172.7	8.1	143.9	4.1	153.3	1.2	159.6
40	212.53	0.12	212.12	0.07	212.27	0.02	212.32	3.576	0.34	3.579	0.20	3.578	0.06	3.577	170.1	8.5	142.1	4.2	151.3	1.3	157.7
41	208.56	0.13	208.17	0.08	208.31	0.02	208.35	3.577	0.36	3.585	0.21	3.582	0.06	3.580	167.6	8.5	140.5	4.3	149.4	1.3	156.0
42	204.74	0.13	204.36	0.08	204.50	0.02	204.53	3.581	0.37	3.590	0.22	3.586	0.06	3.584	165.2	8.6	139.0	4.3	147.6	1.3	154.3
43	201.06	0.13	200.67	0.08	200.81	0.02	200.85	3.585	0.40	3.595	0.24	3.591	0.07	3.588	162.9	8.8	137.6	4.4	146.0	1.3	152.7
44	197.50	0.14	197.12	0.08	197.26	0.02	197.28	3.589	0.42	3.600	0.25	3.596	0.07	3.593	160.8	8.9	136.3	4.5	144.4	1.4	151.2
45	194.06	0.14	193.68	0.09	193.82	0.02	193.84	3.591	0.47	3.607	0.27	3.601	0.08	3.597	160.2	9.4	134.8	4.7	143.1	1.4	149.7
46	190.73	0.15	190.34	0.09	190.48	0.03	190.51	3.594	0.49	3.615	0.29	3.607	0.08	3.602	158.4	9.8	133.8	4.9	141.8	1.5	148.3
47	187.57	0.15	187.11	0.09	187.27	0.03	187.29	3.596	0.52	3.621	0.31	3.612	0.09	3.606	158.8	10.2	132.4	5.0	140.9	1.6	146.9
48	184.43	0.16	184.01	0.09	184.17	0.03	184.18	3.603	0.56	3.625	0.33	3.617	0.10	3.611	153.3	10.1	133.8	5.2	140.4	1.6	145.7
49	181.41	0.16	180.99	0.10	181.15	0.03	181.16	3.608	0.60	3.631	0.35	3.623	0.10	3.615	151.5	10.3	133.0	5.4	139.3	1.6	144.4
50	178.43	0.17	178.12	0.11	178.24	0.03	178.24	3.619	0.62	3.631	0.38	3.626	0.11	3.620	154.6	10.9	129.0	5.6	137.5	1.7	143.2
51	175.60	0.18	175.28	0.11	175.40	0.03	175.40	3.622	0.65	3.637	0.40	3.631	0.11	3.624	152.8	11.2	128.4	5.8	136.5	1.7	142.1
52	172.87	0.18	172.54	0.11	172.66	0.03	172.65	3.626	0.60	3.641	0.36	3.635	0.10	3.629	152.7	12.1	126.9	6.0	135.4	1.9	140.9
53	170.20	0.19	169.87	0.11	169.99	0.03	169.98	3.629	0.62	3.647	0.37	3.640	0.11	3.633	151.5	12.4	126.2	6.2	134.5	1.9	139.9
54	167.54	0.22	167.35	0.13	167.42	0.04	167.39	3.646	0.75	3.646	0.44	3.646	0.12	3.637	159.6	15.0	124.5	6.8	135.3	2.1	138.8
55	165.02	0.22	164.83	0.13	164.90	0.04	164.88	3.649	0.79	3.652	0.46	3.651	0.13	3.641	158.6	15.4	123.9	7.0	134.5	2.2	137.8

The results for 'pure path' Q indicate that the derived differences are not statistically significant; there is some indication, however, that Q for the continental regions may be higher than for the oceanic ones. We test this hypothesis by decreasing the resolution of the regionalization and distinguishing only between continents and oceans. The results are shown in Table 3, which also contains the properly weighted global average and comparison with the appropriate functionals for PREM (Dziewonski & Anderson 1981). The standard errors in 'pure path' Q decrease substantially and could be considered statistically significant. The systematic trend of differences between the continental and oceanic Q values is illustrated in Fig. 13. At a period of 250 s the continental and oceanic Q's are 196 ± 16 and 160 ± 7, respectively – a difference of about 20 per cent. The lower Q for the oceans obtained in this study is in agreement with the results of Sipkin & Jordan (1980) based on measurements of Q of *ScS* reflections.

The comparison of the average data from 37 paths studied in this paper with the functionals of PREM, a model derived using a much broader data base, is a test of the overall performance of WIT. Even small systematic differences could be detected in this way. For periods of normal modes, the maximum difference is 0.05 per cent with an average rms of 0.02 per cent, an excellent agreement indeed. The differences between the group velocities do not significantly exceed 0.01 km s^{-1} – a remarkable result considering the fact that group velocities were not used in derivation of PREM and that there are substantial variations in group velocities estimated for individual paths: the maximum difference in 'pure path' group velocities approaches 5 per cent. The average Q values are also very close to those for PREM.

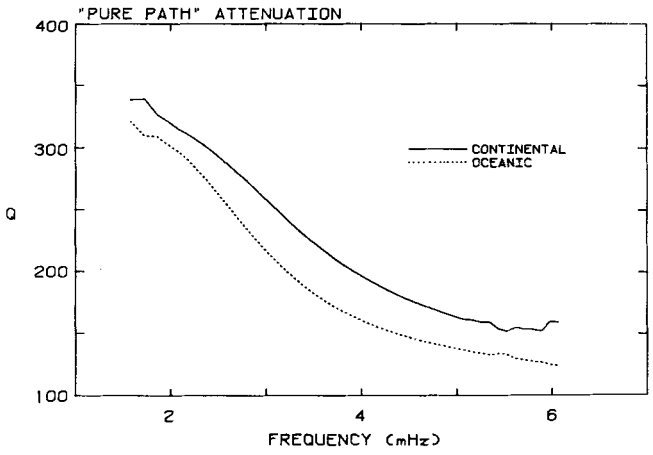

Figure 13. Attenuation (Q) for continental and oceanic regions; the data are not sufficiently numerous and accurate to allow the four region analysis for Q. However, inspection of Table 2 reveals that the continental Q values are generally higher than the oceanic ones. The results shown in the figure have been obtained by combining the tectonic and stable continental regions on one hand and young and old oceans on the other. The differences between the continental and oceanic Q values are statistically significant; see Table 3.

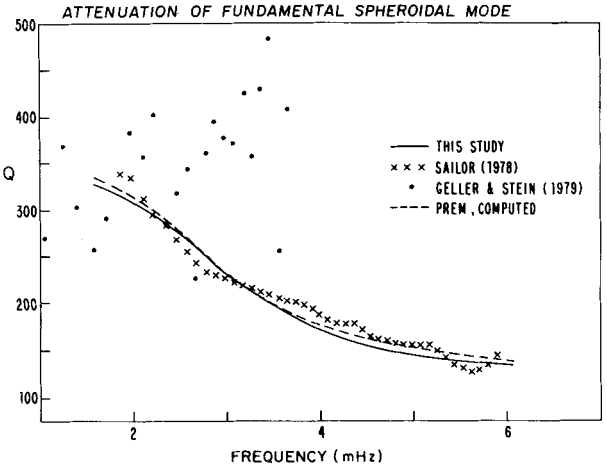

Figure 14. Comparison of Q data of Sailor (1978; travelling wave approach), Geller & Stein (1979; standing wave approach) with those obtained in this study; values computed for PREM (Dziewonski & Anderson 1981) are added for reference.

At all frequencies the differences are less than 5 per cent, which is the estimated accuracy of the average Q data in the relevant range of frequencies (see table V of Dziewonski & Anderson 1981).

Because of the inherent difficulty in the direct comparison of the results of measurements of Q with the original data (seismograms), we show in Fig. 14 the average Q values obtained in this study together with the results of Sailor (1978) and Geller & Stein (1979); the Q curve for PREM is included. Sailor obtained his results by using the travelling wave approach and a refined spectral ratio method, thus there should be no common source of bias between his results and ours. Sailor's data show small amplitude oscillations superimposed on a

smooth curve that is essentially parallel to ours with a few per cent systematic difference at the short period end. The results of Geller & Stein, obtained by measuring the time domain decay of the envelope of individual modes, have very large scatter; this might be construed as an indication of the advantage of the travelling wave approach for periods shorter than about 500 s.

Finally, we consider the results obtained in the model space. For each path we have a set of perturbations in velocities and Q that were introduced to improve the transfer function. We can, thus, modify equation (12) by substituting v or $1/Q$ for ω and solve for the 'pure path' models. As stated above, the results need not be fully compatible with those obtained for the normal mode functionals, because the frequency range of inversion differs from path to path, while the parametrization remains the same. Also, the models of the crust, lithosphere and low velocity zone are clearly inappropriate for the individual regions. Our regional structures are obtained by inverting for the first-order perturbations to an average earth model. Therefore, the geophysical significance of these models may be open to question. In accordance with the experience gained from the analysis of synthetic data (Section 3, Figs 1–5), the primary objective of our pure 'pure path' analysis is to derive the transfer functions. Refinement of the model space results for regionalized structures is rather involved and should be the subject of a separate study. In the next section we outline briefly how this could be achieved.

Fig. 15 shows perturbations in shear velocity for the individual regions with respect to the reference model (IREM). The most unusual feature of this plot are the large differences between the velocities for young and old oceans in a depth range from 400 to 670 km. At shallower depths, the results are compatible with those from other studies. The structures in the depth range from 80 to 220 km reflect the composite properties of the crust, lithosphere and the low velocity zone: fundamental Rayleigh mode data with a short-period cut-off at 165 s have no resolving power to determine these separate elements of the structure.

The total spread of values is very large (0.34 km s^{-1}) in the depth range from 80 to 220 km. The relative slowness of the young oceans and tectonic regions is in good agreement with regional surface wave studies. The total spread of shear velocities is relatively small in the depth range from 220 to 400 km. It is less than 0.1 km s^{-1}, and the error bars indicate that the differences are not statistically significant. In a depth range from 400 to 670 km the velocities for stable continents and tectonic regions are very close to each other and, also, to

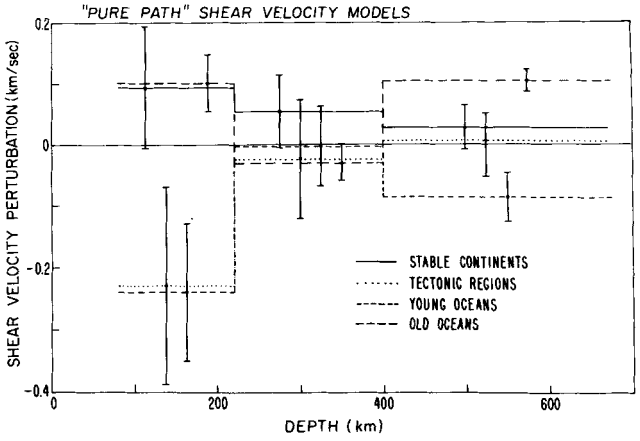

Figure 15. 'Pure path' shear velocity models obtained through decomposition of structural parameters derived for each of 37 analysed seismograms; bars indicate the standard errors.

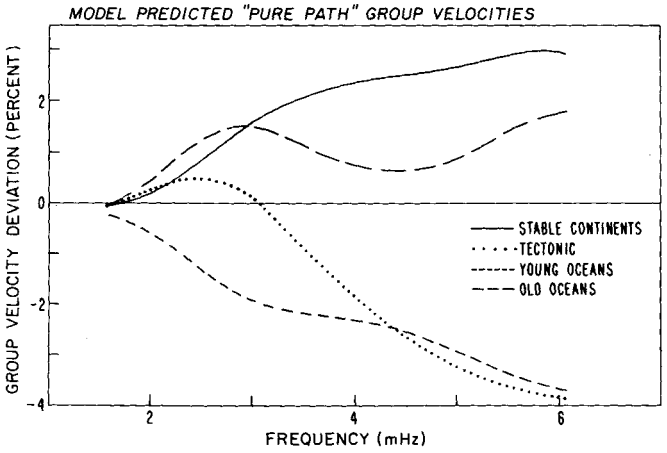

Figure 16. Group velocities computed for the models shown in Fig. 15. Because the range of frequencies for which measurements were made varied from record to record, the models obtained through decomposition need not be fully compatible with the 'pure path' data. Comparison of this figure with Fig. 12(b) indicates, however, that all major features are similar for both figures.

the global average. The difference between the young and old oceans is large: nearly 0.2 km s^{-1} or 4 per cent, and appears to be statistically significant. One cannot discount the possibility that it is an artefact of the errors introduced by the geometrical ray theory approximation, but in that case abnormal properties of the models for stable continents and tectonic regions could be expected: either of these two region types is smaller in the total area than the young or old oceans.

Variation in size of the error bars may be indicative of either real or apparent spread of velocities within a given type of region and a particular depth range. For example, the very large error bar for the 80–220 km depth range of the tectonic model could be interpreted as an expression of non-uniformity of structures within this classification. This is not surprising if one recalls that we label as 'tectonic' island arcs as well as young mountainous regions.

To check that our 'pure path' models are consistent with the 'pure path' data we calculate exactly the functionals for the models shown in Fig. 15. The results for the group velocities are shown in Fig. 16. There are small differences between this figure and Fig. 12(b), but the overall character of the curves in both figures is the same.

5 Discussion

Our method of waveform inversion technique (WIT) yields reliable results for mantle Rayleigh waves in a range of periods from 160 to 600 s. This has been demonstrated for both dispersion and attenuation through a series of experiments with synthetic and actual data. Experiments with the actual data involved comparisons of dispersion measurements using WIT and phase delay methods for individual source-station pairs. They also included processing of a large data set (37 paths). The global average values derived from the latter experiment compare favourably with the dispersion and attenuation data obtained by other methods as well as with the functionals predicted by the Preliminary Reference Earth Model of Dziewonski & Anderson (1981). Thus, it appears that the results obtained using WIT are not burdened by a discernible systematic bias.

A conceptually novel, and not yet fully exploited, aspect of the method is the establishment of the direct relationship between the waveform data and the model space. In the future this property of WIT can be used to combine in a single inversion Rayleigh and Love wave data from a given source region to a particular station. The problem of 'pure path' or 'local' structures could be formulated directly in the model space and, indeed, it appears that the application of the theory of Woodhouse & Girnius (1982) will be most advantageous in such a formulation. The method can be immediately extended to the problem of measurement of phase velocities and attenuation between two stations in the classical two-station method, as the problem here is also that of determination of the transfer function. A more indirect and much more complex application is to the multi-mode propagation problem. In this case, while the concept of matching the waveforms through perturbations in the model space remains the same, one must incorporate in the model also the seismic source using, for example, the representation of Dziewonski, Chou & Woodhouse (1981). In the long run, such studies should provide an increased level of detail of lateral heterogeneities for a wide range of depths.

The work described here represents only the first step in modelling lateral heterogeneity. In a second step, one should design regional models consistent with 'pure path' dispersion data and, in the sense of a weighted average, also with gross Earth data, such as the periods and Q's of overtones or of the gravest fundamental modes. The procedure could be similar to that used by Dziewonski, Hales & Lapwood (1975) in derivation of PEM-C and PEM-O models. These regional models could then be used as starting models in inversion of waveform data. Inversion would not be performed for individual seismograms, as in this paper, but for an ensemble of records covering many great circle paths. This, if done in several iterations, would allow us to avoid the non-linearity which could have biased our model space results.

The results of the 'pure path' analysis must be considered tentative for reasons stated above and because of the potential source of errors introduced by the geometrical ray theory approximation. The errors can be expected to increase with the wavelength and, except for the study of Silver & Jordan (1981), we have doubled the wavelength in comparison with previous 'pure path' studies.

The matter should be satisfactorily resolved by application of the theory of Woodhouse & Girnius (1982), which avoids the approximation inherent in the geometrical ray theory. Also, improved path coverage should lead to higher resolution. The important result of this experiment is that the extended period range provides sufficient resolution below a depth of 400 km to infer structural differences in the region of the transition zone.

The increased nominal resolution in the range of depths from 400 to 670 km leads to the inference of a major (4 per cent) difference between the shear velocities for young and old oceans at these depths. At the same time, the young oceans are also much slower (0.3 km s^{-1}) in a depth range from 80 to 220 km, while no major differences are inferred for the intermediate depths (220–400 km). It is difficult to resist an analogy with the hot and cold halves of a convection cell.

In order to explain these differences by the effect of temperature alone, the contrast would have to be on the order of 500°C. Perhaps elevation of phase transformations to higher velocities in the colder oceans could contribute to this effect. With the radii of discontinuities held fixed, such changes in elevation would be equivalent to an apparent change in the average velocity.

Rough calculations indicate that the upper mantle S-wave transit time is about the same for our stable continent and old ocean structures, in agreement with the study of multiple ScS reflections by Okal & Anderson (1975). The structures for the stable continents and tectonic regions are very similar to each other in the depth range from 400 to 670 km and

are close to the average structure, even though instability could be expected to be the largest for these regions, because of their small total area. Thus the conceptually important features of our regional models may be considered plausible.

Acknowledgments

The authors wish to thank Professor John H. Woodhouse for his help, numerous discussions and critical reading of the manuscript. In particular, he suggested the transformation used in derivation of equation (11). Professor Raymond Jeanloz provided us with helpful suggestions with respect to the possible nature of the deep seated differences between the structures for young and old oceans. Professor Richard J. O'Connell and two anonymous reviewers provided helpful comments. We would like to thank the entire staff of the IDA project at the Institute of Geophysics and Planetary Physics of the University of California, San Diego, and Professor Freeman Gilbert in particular, for making available to us the tapes with the superb data produced by their network. This research has been supported by a grant EAR77-13661 from the National Science Foundation.

References

Agnew, D., Berger, J., Buland, R., Farell, W. & Gilbert, F., 1976. International deployment of accelerometers: a network for very low frequency seismology, *Eos, Trans. Am. geophys. Un.*, **57**, 180–188.

Backus, G. & Gilbert, F., 1967. Numerical applications of a formalism for geophysical inverse problems, *Geophys. J. R. astr. Soc.*, **13**, 247–276.

Brune, J. N., Nafe, J. E. & Alsop, L. E., 1961. The polar phase shift of surface waves on the sphere, *Bull. seism. Soc. Am.*, **57**, 247–257.

Dahlen, F. A., 1975. The correction of great circular surface wave phase velocity measurements for the rotation and ellipticity of the Earth, *J. geophys. Res.*, **80**, 4895–4903.

Dziewonski, A. M., 1971. On regional differences in dispersion of mantle Rayleigh waves, *Geophys. J. R. astr. Soc.*, **22**, 289–325.

Dziewonski, A. & Anderson, D. L., 1979. *A Proposal for an Interim Reference Earth Model*, unpublished report submitted to the Standard Earth Model Committee of the IUGG, Canberra, Australia.

Dziewonski, A. & Anderson, D. L., 1981. Preliminary reference earth model, *Phys. Earth planet. Int.*, **25**, 297–356.

Dziewonski, A., Chou, T.-A. & Woodhouse, J. H., 1981. Determination of earthquake source parameters from waveform data for studies of global and regional seismicity, *J. geophys. Res.*, **86**, 2825–2852.

Dziewonski, A. M., Hales, A. L. & Lapwood, E. R., 1975. Parametrically simple earth models consistent with geophysical data, *Phys. Earth planet. Int.*, **10**, 12–48.

Dziewonski, A. & Landisman, M., 1970. Great circle Rayleigh and Love wave dispersion from 100 to 900 seconds, *Geophys. J. R. astr. Soc.*, **19**, 37–91.

Dziewonski, A., Mills, J. & Bloch, S., 1972. Residual dispersion measurement – a new method of surface waves analysis, *Bull. seism. Soc. Am.*, **62**, 129–139.

Dziewonski, A. M. & Sailor, R. V., 1976. Comments on "The correction of great circular surface wave phase velocity for the rotation and ellipticity of the Earth" by F. A. Dahlen, *J. geophys. Res.*, **81**, 4947–4950.

Geller, R. J. & Stein, S., 1979. Tome-domain attenuation measurements for fundamental spheroidal modes ($_0S_6$ to $_0S_{28}$) for the 1977 Indonesian earthquake, *Bull. seism. Soc. Am.*, **69**, 1671–1691.

Jordan, T. H., 1978. A procedure for estimating lateral variations from low frequency eigenspectra data, *Geophys. J. R. astr. Soc.*, **52**, 441–455.

Kanamori, H., 1970. Velocity and Q of mantle waves, *Phys. Earth planet. Int.*, **2**, 259–275.

Knopoff, L., 1972. Observation and inversion of surface wave dispersion, *Tectonophys.*, **13**, 497–519.

Lévêque, J. J., 1980. Regional upper mantle S-velocity models from phase velocities of great-circle Rayleigh waves, *Geophys. J. R. astr. Soc.*, **63**, 23–43.

Liu, H.-P., Anderson, D. L. & Kanamori, H., 1976. Velocity dispersion due to anelasticity: implications for seismology and mantle composition, *Geophys. J. R. astr. Soc.*, **47**, 41–58.

Mauk, F. J., 1977. A tectonic based Rayleigh wave group velocity model for production of dispersion character through ocean basins, *PhD thesis*, University of Michigan.

Nakanishi, I., 1979. Phase velocity and Q of mantle waves, *Geophys. J. R. astr. Soc.*, **58**, 35–59.

Nakanishi, I., 1981. Shear velocity and shear attenuation models from world-wide and pure-path average data of mantle Rayleigh waves ($_0S_{25}$ to $_0S_{80}$) and fundamental spheroidal modes ($_0S_2$ to $_0S_{24}$), *Geophys. J. R. astr. Soc.*, **66**, 83–130.

Okal, E. A. & Anderson, D. L., 1975. A study of lateral heterogeneities in the upper mantle by multiple *ScS* travel time residuals, *Geophys. Res. Lett.*, **2**, 313–316.

Sailor, R. V., 1978. Attenuation of low frequency seismic energy, *PhD thesis*, Harvard University.

Satō, Y., 1958. Attenuation, dispersion and the wave guide of the *G* wave, *Bull. seism. Soc. Am.*, **48**, 231–251.

Silver, P. G. & Jordan, T. H., 1981. Fundamental spheroidal mode observations of aspherical heterogeneity, *Geophys. J. R. astr. Soc.*, **64**, 605–634.

Sipkin, S. A. & Jordan, T. H., 1980. Regional variations of Q_{ScS}, *Bull. seism. Soc. Am.*, **70**, 1071–1102.

Toksöz, M. N. & Anderson, D. L., 1966. Phase velocities of long period surface waves and structure of the upper mantle, *J. geophys. Res.*, **71**, 1649–1658.

Woodhouse, J. H. & Girnius, T. P., 1982. Surface waves and free oscillations in a regionalized earth model, *Geophys. J. R. astr. Soc.*, **68**, 653–673.

Wu, F. T., 1972. Mantle Rayleigh wave dispersion and tectonic provinces, *J. geophys. Res.*, **77**, 6445–6453.